MR Imaging-Histopathologic Correlation of Radiofrequency Thermal Ablation Lesion in a Rabbit Liver Model: Observation during Acute and Chronic Stages

Jong Deok Lee, MD[1, 2]
Jeong Min Lee, MD[1]
Sang Won Kim, MD[1]
Chong Soo Kim, MD[1]
Woo Sung Mun, MD[3]

Objective: To determine the ability of MR imaging to detect the pathological changes occurring in radiofrequency (RF) thermal lesions and to assess its accuracy in revealing the extent of tissue necrosis.

Materials and Methods: Using an RF electrode, thermal lesions were created in the livers of 18 rabbits. The procedure involved three phases. In the acute phase, six animals were killed the day after performing thermal ablation with RF energy, and two on day 3. In the subacute and chronic phases, eight rabbits underwent percutaneous hepatic RF ablation. After performing MR imaging, two animals were sacrificed at 1, 2, 4, and 7 weeks after the procedure, and MR-pathologic correlation was performed.

Results: In the acute phase, the thermal ablation lesions appeared at gross examination as well-circumscribed, necrotic areas, representing early change in the coagulative necrosis seen at microscopic examination. They were hypointense on T2-weighted images, and hyperintense on T1-weighted images. Gadolinium-enhanced MR imaging showed that a thin hyperemic rim surrounded the central coagulative necrosis. In the subacute phase, ablated lesions also showed extensive coagulative necrosis and marked inflammation at microscopic examination. Beyond two weeks, the lesions showed gradual resorption of the necrotic area, with a peripheral fibrovascular rim. The size of lesions measured by MR imaging correlated well with the findings at gross pathologic examination.

Conclusion: MR imaging effectively demonstrates the histopathological tissue change occurring after thermal ablation, and accurately determines the extent of the target area.

Index terms:
Liver, MR
Liver, interventional procedure
Interventional procedures, experimental

Korean J Radiol 2001;2:151-158
Received February 19, 2001; accepted after revision July 12, 2001.

Department of Diagnostic [1]Radiology and [3]Surgical Pathology, Chonbuk National University Medical School; Department of [2]Diagnostic Radiology, Kwangju Wonkwang Hospital

Address reprint requests to:
Jeong-Min Lee, MD, Department of Diagnostic Radiology, Chonbuk National University Hospital, 634-18 Keumam-dong, Chonju-shi, Chonbuk 561-712, South Korea.
Telephone: (8263) 250-1176
Fax: (8263) 272-0481
e-mail: jmsh@chonbuk.ac.kr

Image-guided, percutaneous ablative therapies using thermal energy sources such as radiofrequency (RF) (1–3), microwave (4) and laser (5) are rapidly evolving as minimally invasive techniques for the treatment of primary and metastatic hepatic tumors. The potential benefits of these techniques over conventional surgical options include tumor ablation in nonsurgical candidates, reduced morbidity compared with surgery, and use of the procedure on an outpatient basis (6). Preliminary clinical reports have demonstrated that hepatic RF ablation produces effective local disease control in a significant proportion of patients with nonresectable liver tumors (7–9). However, according to even the most optimistic long-term report of percutaneous RF thermal therapy in colorectal metastases, local tumors recurred in 35% of cases (10). In addition, recent studies have shown that a significant proportion of patients with hepatocellular carcinomas greater than 3–5 cm in diameter experienced local recurrence after the use of current thermal ablation strategies (11–12).

When lesions appear to have been successfully treated, it is very important to detect any areas of untreated or local tumor recurrence at an early stage: failure to identify a small residual or recurrent tumor leads to peripheral regrowth. Although contrast-enhanced CT is probably the most widely used technique for the follow-up of treated lesions (3, 11, 13), a difficulty often arises with small recurrent or residual tumors. A few recent reports have addressed the use of follow-up MR imaging after RFA application (14, 15). High sensitivity to tissue water distribution and temperature as well as high soft-tissue contrast make MR imaging the most attractive imaging tool for the assessment of RFA-induced thermal tissue damage. There has, however, been a lack of detailed MR imaging-histopathologic correlations (14, 15).

The purpose of this investigation was to evaluate the potential of MR imaging in revealing the extent of true tissue necrosis and to determine the dynamics of thermal injury in an acute and chronic animal model using MR imaging-histopathologic correlation.

MATERIALS AND METHODS

Eighteen New Zealand White rabbits (male, 2.5−3 kg) were anesthetized by intramuscular injection of 50 mg/kg ketamine hydrochloride (Ketamine; Yuhan, Seoul, Korea) and 5 mg/kg of xylazine (Rompun; Bayer Korea, Ansan, Korea). After adequate anesthesia was achieved, the epigastrium and back were shaved and sterilized, and a wire mesh ground pad and conductive gel were placed on the animal's back. An internally cooled, 18-gauge electrode (Radionics, Burlington, Mass., U.S.A.) with a 1−2 cm active tip was inserted into the liver of each animal under ultrasound guidance (Sequoia; Acuson, Mountain View, Cal., U.S.A.) using a 10-MHz probe.

Lesions were created using a 500-kHz RF generator (series CC-3; Radionics, Burlington, Mass., U.S.A.) capable of producing 200W of power. During the procedure, a thermocouple embedded within the electrode tip continuously measured local tissue temperature. Tissue impedance was monitored by circuitry incorporated into the generator. A peristaltic pump (Watson-Marlow, Medford, Mass., U.S.A.) was used to infuse normal saline solution at 0°C into the lumen of the electrodes at a rate sufficient to maintain a tip temperature of 20−25°C. Power output was set at 30 W and RF energy was applied for approximately 3 minutes, or until lesions of approximately 1×2 cm were produced.

MR imaging was performed with a 1.5-T instrument (Vision; Siemens Medical Systems, Erlangen, Germany) within 2 hours of RF ablation (day 1), on day 3, and at 1, 2, 4, and 7 weeks. Transverse conventional spin-echo and gradient-echo T1-weighted (T1WI) and turbo spin-echo T2-

Table 1. Summary of MR Imaging and Histopathologic Findings of Radiofrequency Thermal Ablated Lesions

Phase	T1WI	T2WI	CE-T1WI	Gross Findings	Microscopic Findings
Acute (n=8)					
Zone 1	Hypointense	Hyperintense	NE	Dark brown-colored needle tract	Tissue loss area, sometimes occupied by fibrin and hemorrhage
Zone 2	Hyperintense	Hypointense	NE	Pale tan zone	Degenerated, swollen hepatocytes with pyknotic nuclei
Zone 3	Isointense	Hyperintense	Enhancing rim	Pinkish, hemorrhagic rim	Sinusoidal congestion
Subacute (n=4)					
Zone 1	Isointense	Hyperintense	NE	Needle tract	Tissue loss area with coagulation necrosis
Zone 2	Center: isointense Outer area: hyerintense	Hypointense	NE	Light yellow zone	Coagulation necrosis
Zone 3	Hypointense	Hyperintense	Enhancing rim	Light gray, thin capsule	Fibrovascular restoration with inflammatory infiltration
Chronic (n=4)					
Zone 1	Isointense	Hyperintense	NE	Dark brown-colored needle tract	Tissue loss area and coagulation necrosis
Zone 2	Center: isointense Outer area: hyerintense	Hypointense	NE	Yellow-to-light gray zone	Coagulation necrosis
Zone 3	Hypointense	Hyperintense	Enhancing rim	Gray-to-white fibrous capsule	Dense mature fibrous tissue

Note.— NE=no enhancement, n=number of rabbits, T1WI=T1-weighted image, T2WI=T2-weighted image, CE-T1WI=contrast-enhanced T1-weighted image

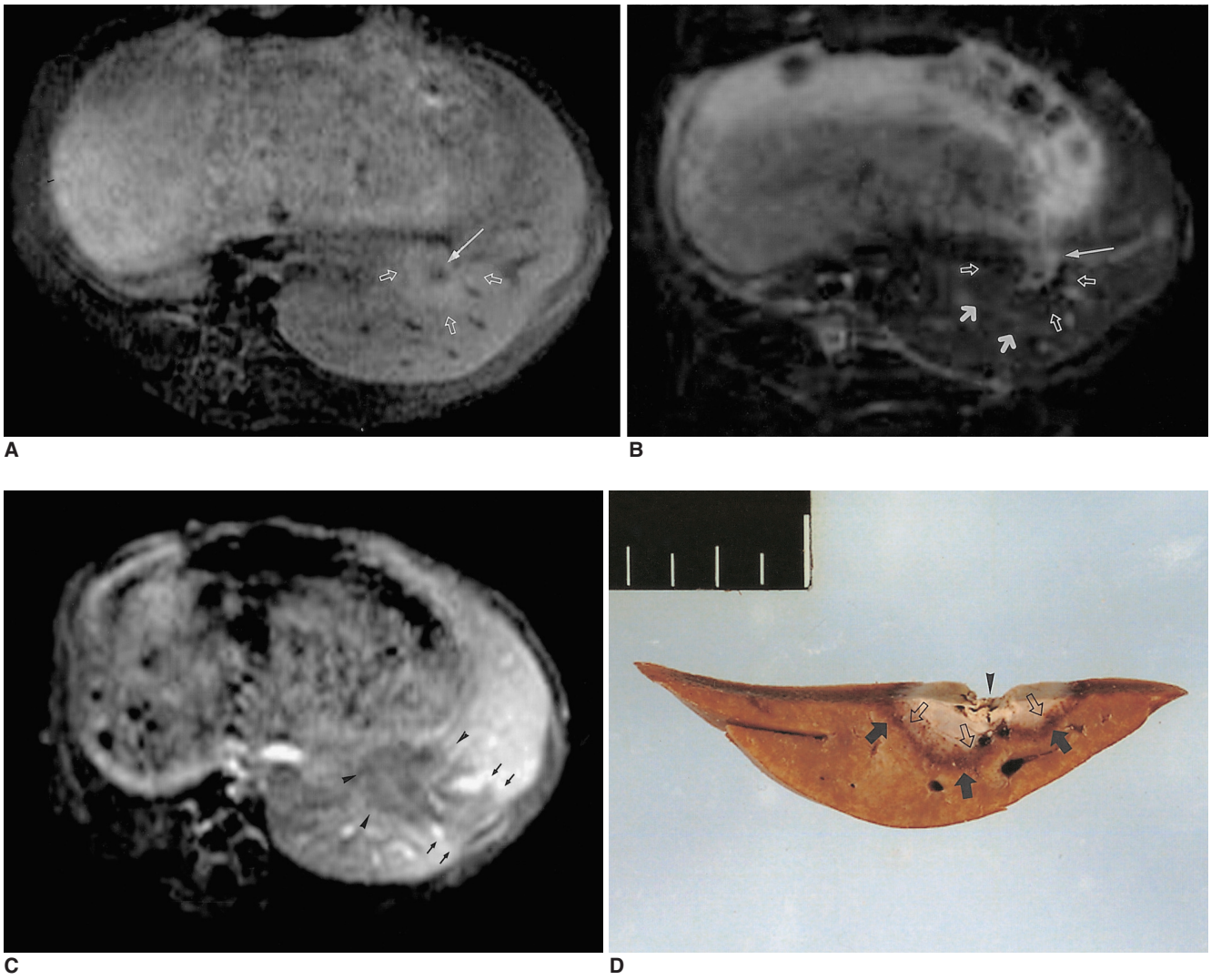

Fig. 1. MRI and histopathologic findings immediately after RF thermal ablation.
A. Gradient-echo T1-weighted image (TR/TE/FA, 153/5/90°) shows an ill-defined hyperintense lesion (open arrows) with a central hypointense spot (arrow).
B. Turbo spin-echo T2-weighted image (TR/TE/NEX/ETL, 24000/99/4/11) demonstrates three zones, with a central hyperintense spot due to blood at the site of needle insertion (thin arrow), a hypointense thermally ablated lesion (open arrows), and a poorly demarcated hyperintense peripheral zone (thick arrows).
C. Contrast-enhanced T1-weighted image (TR/TE/Nex, 153/5/2) depicts an RF thermal lesion as a hypointense perfusion defect area (arrowheads). There is a wedge-shaped perfusion abnormality adjacent to the ablated lesion (small arrows).
D. Cut gross specimen demonstrates a central white cavity of tissue loss (arrowhead) and a wider zone of pale liver tissue (open arrows) surrounded by a small hemorrhagic rim (arrows), with normal liver peripherally.
E. Microscopic examination reveals the area of the ablated lesion. Zone 2 indicates a wider zone of early necrosis (N), and zone 3, congestion and sinusoidal hemorrhage of the liver (H). Normal liver parenchyme (L) surround the lesion peripherally (hematoxylin-eosin stain; original magnification, ×20).

weighted images (T2WI) were obtained using 4-mm section thickness, 1-mm intersection spacing, and a 20 ×16-cm field of view. Four signals were acquired. For T1-weighted spin-echo images, a repetition time of 405 msec, an echo time of 12 msec (405/12) and a matrix of 256 ×125 were used. For T2-weighted turbo spin-echo images (2400/99), the echo train length was 11 and the matrix was 256 ×132. Nonenhanced and dynamic contrast-enhanced T1-weighted fast multiplanar spoiled gradient-echo images (153/5, 90°) were obtained with 4-mm section thickness, 1-mm intersection spacing, 256 ×96 matrices and a 20 ×16-cm field of view. Acquisitions were made 0, 30, 60, 120 and 180 seconds after bolus intravenous administration of 0.1 mmol/kg gadopentetate dimeglumine (Magnevist; Schering, Berlin, Germany).

Six rabbits were killed on the day after the procedure, and two on day 3 and at 1, 2, 4, and 7 weeks. On day three and four, two animals died of peritonitis due to delayed perforation of the stomach by accidental ablation. Other animals were killed using a barbiturate overdose technique and their livers were harvested prior to gross examination. A central cross-sectional incision was made through the affected area, and a 5-mm parallel section was obtained from the lesion. For macroscopic pathologic analysis, the central discolored region of coagulation necrosis was measured with calipers in each pathologic specimen. Measurements of the diameter of coagulation perpendicular to the electrode axis were based upon the consensus of two observers. Tissues were then fixed in 10% phosphate-buffered formalin for routine histologic processing; specimens from all treatment areas were analyzed for nonviability, histologic appearance, and demarcation from surrounding viable tissue. Lesion size at MRI was determined by caliper measurement from printed images before and after administration of the contrast agent by the other examiner, who was blinded to the results of measurement of the gross specimen. Lesion size was measured twice, at pathologic examination and at MRI, and an average was then computed.

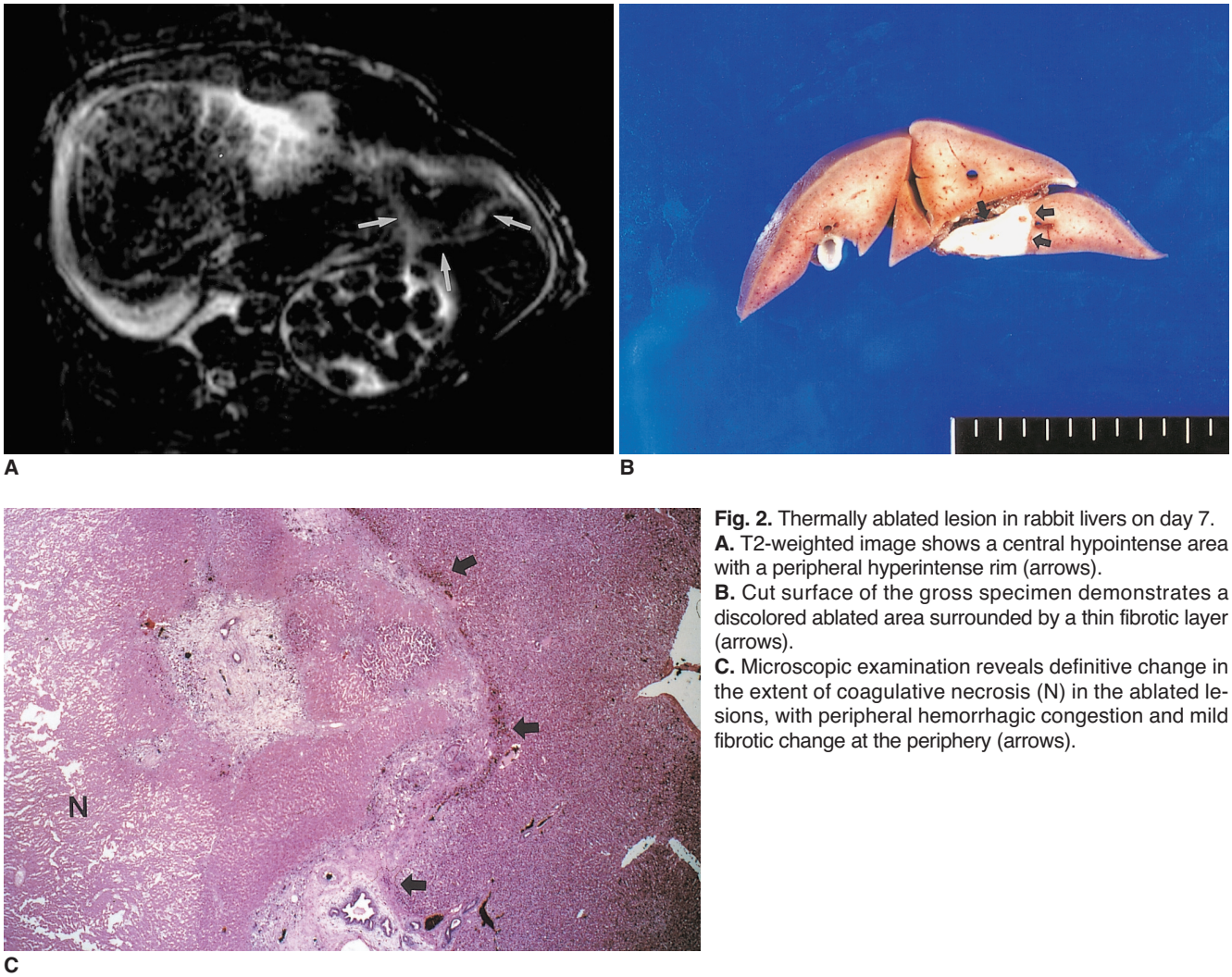

Fig. 2. Thermally ablated lesion in rabbit livers on day 7.
A. T2-weighted image shows a central hypointense area with a peripheral hyperintense rim (arrows).
B. Cut surface of the gross specimen demonstrates a discolored ablated area surrounded by a thin fibrotic layer (arrows).
C. Microscopic examination reveals definitive change in the extent of coagulative necrosis (N) in the ablated lesions, with peripheral hemorrhagic congestion and mild fibrotic change at the periphery (arrows).

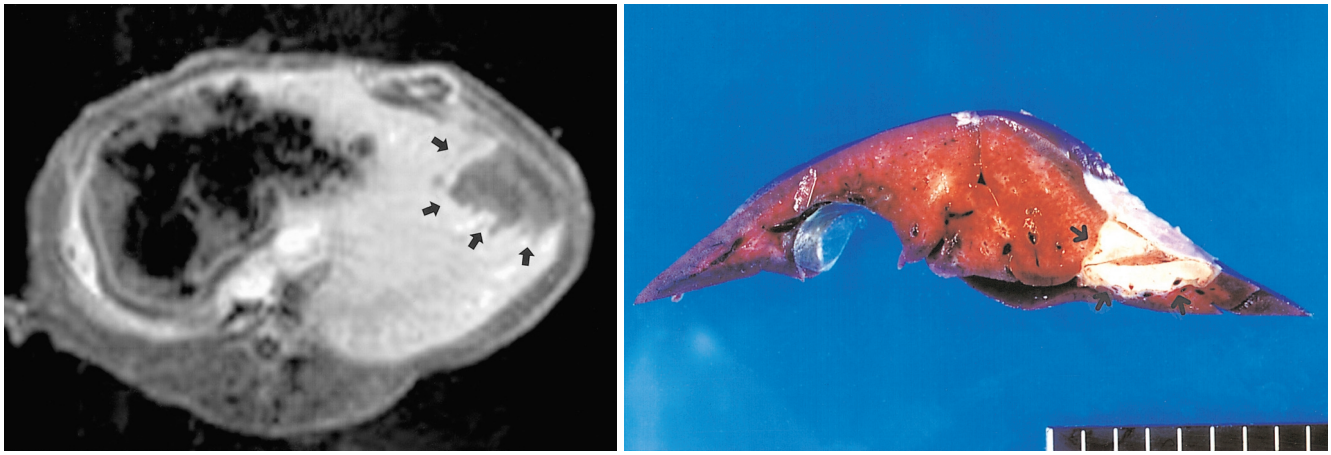

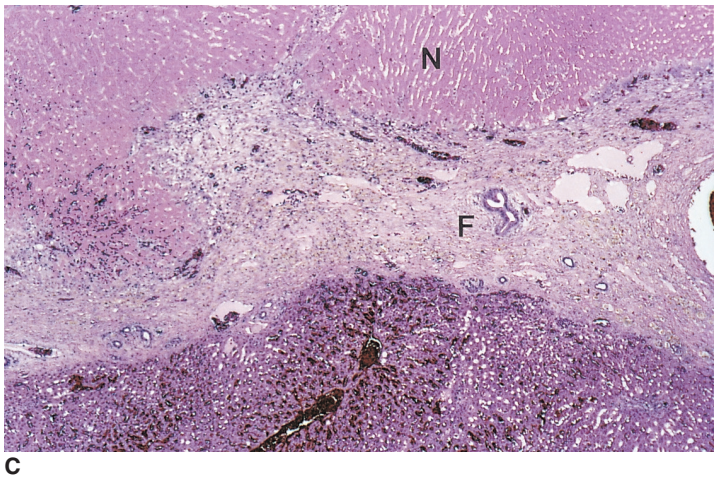

Fig. 3. MR and pathologic findings two weeks after RF ablation.
A. Contrast-enhanced T1-weighted image depicts a well-demarcated hypointense lesion surrounded by a thick enhancing rim (arrows).
B. Cut surface of the gross specimen shows a well demarcated, wedge-shaped, pale area with fibrotic capsule formation (arrows).
C. Microscopic examination reveals central coagulative necrosis (N), with a thick rim of peripheral fibrotic capsule (F) infiltrated by chronic inflammatory cells (hematoxylin-eosin stain; original magnification ×20).

The size of the hyperintense core seen at T1WI, the hypointense core at T2WI and the nonenhancing lesion at contrast-enhanced T1WI (CE-T1WI) was correlated with the lesion size determined at pathologic examination, and then analyzed using Pearson's correlation coefficient, which was used to describe the degree of correlation between all possible two-variable comparisons. Statistical significance was established using Student's two-tailed t test.

Table 2. Correlation Coefficients and Mean Diameter of Radiofrequency Thermal Lesions as Observed at MR Imaging and Compared with Gross Pathology

	Mean diameter (mm)	Correlation coefficient
Gross pathology	20.7±7	–
T1-weighted image	19±5	0.74
T2-weighted image	18.6±6	0.85
Contrast-enhanced T1-weighted image	22±6	0.92

Note.— Average ±standard deviation

RESULTS

RF ablation created 18 lesions, but since two rabbits died of peritonitis, MR imaging-histopathologic correlation was possible in only 16 of these. Acute-phase MRI of ablated lesions revealed three zones (Fig. 1): (a) zone 1, a central zone showing high-SI at T2WI and low SI at T1WI, and corresponding to the area of tissue loss revealed by histopathologic examination; (b) zone 2, a broad zone showing low SI at T2WI and high SI at T1WI, with lack of enhancement at contrast enhanced (CE)-T1WI and corresponding to the coagulative necrosis seen at histopathologic examination; (c) zone 3, in which hyperintensity was demonstrated by T2-weighted imaging, and isointensity by T1-weighted. In addition, a peripheral enhancing rim-corresponding to hemorrhagic rim macroscopically, and histopathologically to an area of sinusoidal congestion-was seen at CE-T1WI to surround the central nonenhancing area. In the acute phase, MR appearances and gross findings of the lesions were similar to those of the hyperacute phase.

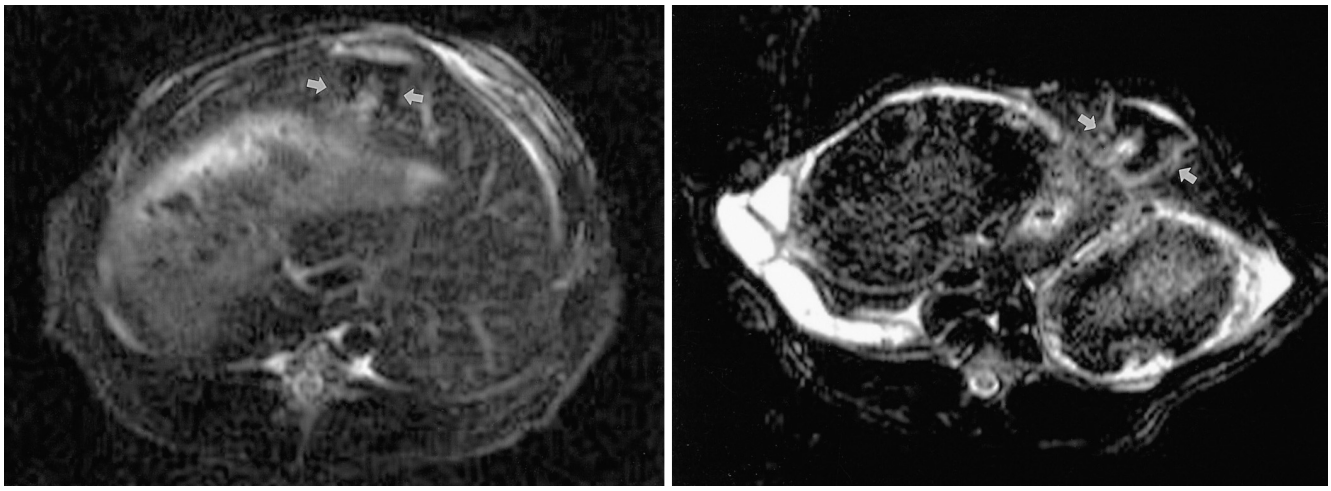

Fig. 4. Sequential changes in MR imaging findings in RF thermal lesions.
A (Day 1), **B** (week 1), and **C** (week 4). T2-weighted images show that the extent of the area of low SI (arrows), corresponding to coagulative necrosis, increased during week 1 and thereafter gradually decreased.

In the subacute phase, MR imaging of the lesions revealed three concentric zones (Figs. 2, 3): (a) zone 1, in which no substantial change was observed, compared with the acute phase; (b) zone 2, in which a broad hypointense zone, corresponding to coagulative necrosis, was seen at T2WI. At T1WI, however, the inner portion became isointense but the outer portion was still hyperintense. Histopathologically, zone 2 contained completely coagulated tissue with no viable cells, and at T1WI, there was no histopathologic difference between the isointense inner portion and the hyperintense outer portion; (c) zone 3, in which a well-defined peripheral hyperintense rim was observed at T2WI, and hypointensity at T1WI. Enhancement corresponding to inflammatory infiltration and fibrovascular restoration was demonstrated by CE-T1WI. In the restoration zone, infiltration by neutrophils and lymphocytes was seen at 1 week, and there was subsequent infiltration by macrophages.

In the chronic phase, MR imaging patterns were similar to those of the subacute phase, but the lesions were smaller (Fig. 4). In this phase, zone 3 (thick peripheral rim) was seen at CE-T1WI to be thicker than in the subacute phase. The diameter of zone 2 (coagulation necrosis) decreased gradually during the chronic phase.

Gross examination showed that lesion diameter, corresponding to the central discolored region, ranged from 10 to 28 (mean, 21) mm and the thickness of the peripheral rim was 1-2 mm. At T2WI, the diameter of thermal lesions, determined in their central hypointense zone, was 10- 28 (mean, 18.6) mm. At T1WI, lesion diameter, measured in the central hyperintense zone, was 9-27(mean, 19) mm, while at CE-T1WI, the diameter, corresponding to the central hypointense nonenhancing zone, was 11-29 (mean, 22) mm. The maximum difference between lesion size on MR images and macroscopic coagulation necrosis was 3 mm. Correlation between the diameter of coagulation necrosis and lesion size at MRI was strong, with the correlation coefficient ranging from 0.74 in the case of T1WI and 0.85

for T2WI, to 0.92 for CE-T1WI ($p<0.05$).

DISCUSSION

Imaging-guided percutaneous tumor ablation using RF energy has been accepted as a minimally invasive strategy for the treatment of focal malignant liver disease (1−3, 6−10). Diagnostic imaging is used not only to guide probe placement but also to monitor the effect of therapy. Although ultrasonography is the predominant imaging technique used for guiding the RF ablation of liver tumors, the accuracy of ultrasonography in depicting the extent of ablated tissue is controversial. Most investigators have relied on contrast-enhanced CT for this purpose (11−13,16−21), though the normal CT appearance of lesions on day 1-7 after RF ablation is that of a low-attenuating lesion, and rim enhancement may be observed (7−13). This appearance may be similar to that of hepatic tumors, and early detection of residual tumor at the RF ablation site is therefore difficult. Rossi et al. recently reported that MR imaging is useful for evaluating the effectiveness of RF therapy (14). Assessment of the adequacy of this treatment requires, however, an understanding of both the sequential changes seen at MRI and the histologic findings of ablated lesions.

In our study, which attempted to evaluate sequential MR imaging of the thermal injuries caused by RF energy and to correlate MR imaging findings with the pathologic findings, MR images clearly demonstrated created lesions in the acute model and sequential changes in tissue response to RF ablation in the subacute and chronic models. Also, images closely approximated to gross pathologic size. In the hyperacute and acute phases, an ablated lesion showed significantly increased SI on T1-weighted images. The hyperintensity observed after RF ablation may be attributed to a number of factors, including mild desiccation, the effect of protein denaturation, and cellular lysis (22, 23). In specimens obtained at 3-7 days, histopathologic examination demonstrated the classic manifestations of coagulative necrosis throughout a majority of the treated zone, but these findings were not present in specimens obtained immediately after ablation. These differences between MR imaging and histopathologic findings in the hyperacute phase concur with those of previous reports that described the progression of ultrasonographic findings during and after percutaneous RF ablation (8, 24). MR imaging therefore has the potential to depict acute, irreversible thermal damage even before morphologic change is seen at the standard pathologic examination.

The marginal area of a lesion was seen as hypointense to isointense at T1WI, with hyperintensity at T2WI. Darkazanili et al. (23) reported that the peripheral high SI seen at T2WI reflected changes in the bound water fraction. In our study, macroscopic examination of this marginal area showed a hemorrhagic rim with degenerated hepatocytes, sinusoidal congestion, and an accumulation of red blood cells. This zone may, therefore, correspond to a transition zone from inner coagulative necrosis to outer normal hepatic tissue. This result is consistent with those of previous reports showing that the inner part of the hemorrhagic rim represented coagulative necrosis, and the outer part corresponded to fibrovascular rim (24, 25).

In the subacute and chronic phases, SI in previously hyperintense areas became isointense at T1WI at least one week later, though T2WI revealed no change in SI. Histopathologic examination of this area revealed necrotic and fibrotic changes which decreased in volume and might have reduced the amount of free water, thus decreasing the SI. One week later a fibrotic zone had formed around the lesion, and the fibrous capsules were thicker in the chronic model than in the subacute model. This fibrous capsule formation is a restoration mechanism occurring after ablation; extensive biologic assays showed that increased collagen production and increased collagenolytic activity occurred seven days after thermal irradiation and had decreased by day 60 (26).

In the clinical setting, MR imaging of hyperacute and acute ablated lesions may be helpful in making the therapeutic decision as to whether additional RF ablation is necessary, or in determining how much tumor volume remains. In considering the clinical aspects of RF ablation, our results suggest that the low-SI zone seen at T2WI, or the high-SI zone at T1WI, must be larger than the tumor margin if complete necrosis is to be achieved. The SI change in ablated tissue is distinct from the SI pattern usually found in primary hepatocellular carcinoma or metastatic liver tumors.

Our study suffered from certain limitations. First, potential differences between rabbit liver and human liver might affect the ultrasonographic and CT appearances of RF-ablated lesions. Second, the results obtained in healthy rabbit livers might be different to those obtained in cases of hepatocellular carcinoma and metastasis in human liver. In view of the nature of cell degeneration caused by the effect of heat on tissue, we believe, however, that the same results might be seen in both normal hepatocytes and cancer cells. In fact, all MR images of hepatocellular carcinomas showed the same SI changes after RF ablation (14). Although every attempt was made to ensure the validity of size correlation between the MR imaging and pathologic findings, absolute precision was not possible because of the difficulty in obtaining pathologic sections corresponding to the scanning

planes of MR imaging.

In conclusion, MR imaging effectively demonstrates the histopathological tissue change occurring after thermal ablation, and accurately determines the extent of the target area.

Acknowledgements

The authors wish to thank Cheol-Ho Kim, M.D. and Jae-Hyuk Yun for their assistance in animal observation and anesthesia, as well as Dae-Hyun Kim and Hyun-Keun Lee for their outstanding support regarding MR imaging procedures.

References

1. Sanctis JTD, Goldberg SN, Mueller PR. Percutaneous treatment of hepatic neoplasms; a review of current techniques. *Cardiovasc Intervent Radiol* 1998;21:273-96
2. Curley SA, Izzo F, Ellis LM, Vauthey JN, Vallone P. Radiofrequency ablation of hepatocellular cancer in 110 patients with cirrhosis. *Ann Surgery* 2000;232:381-91
3. Curley SA, Izzo F, Delrio P, Ellis LN, et al. Radiofrequency ablation of unresectable primary and metastatic hepatic malignancies: results in 123 patients. *Ann Surgery* 1999;230:1-8
4. Vogl TJ, Muller PK, Hammerstingle R, et al. Malignant liver tumors treated with MR imaging-guided laser-induced thermotherapy: technique and prospective results. *Radiology* 1995; 196:257-265
5. Seki T, Wakabayashi M, Nakagawa T, et al. Ultrasonically guided percutaneous microwave coagulation therapy for small hepatocellular carcinoma. *Cancer* 1994;74:817-825
6. Goldberg SN, Livraghi T, Solbiati L, Gazelle GS. *In situ ablation of focal hepatic neoplasms.* In Gazelle GS, Saini S, Mueller PR, eds. *Hepatobiliary and pancreatic radiology: imaging and intervention.* New York, NY: Thieme, 1997; 470-502
7. Rossi S, Di Stasis M, Buscarini E, et al. Percutneous RF interstitial thermal ablation in the treatment of hepatic cancer. *AJR* 1996;167:759-768
8. Solbiati L, Ierace T, Goldberg SN, et al. Percutaneous US-guided radiofrequency tissue ablation of liver metastases: treatment and follow-up in 16 patients. *Radiology* 1997;202:195-203
9. Goldberg SN, Gazelle GS, Solbiati L. Ablation of liver tumors using percutaneous RF therapy. *AJR* 1998;170:1023-1028
10. Solbiati L, Goldberg SN, Tiziana I, et al. Long-term follow-up of liver metastases treated with percutaneous US-guided radiofrequency (RF) ablation using internally-cooled electrodes (abstr). *Radiology* 1998;209(P):449
11. Livraghi T, Meloni F, Goldberg SN, Lazzaroni S, Solbiati L, Gazelle GS. Hepatocellular carcinoma: radio-frequency ablation of medium and large lesions. *Radiology* 2000;214:761-768
12. Siperstein A, Garland A, Engle K, et al. Local recurrence after laparoscopic radiofrequency thermal ablation of hepatic tumors. *Ann Surg Oncol* 2000;7:106-113
13. Catalano O, Cusati B, Sandomenico F, Nunziata A, and Siani A. Helical CT findings in patients with hepatocellular carcinoma treated with percutaneous ablation procedure. *J Comput Assist Tomogr* 2000;24:748-754
14. Sironi S, Livraghi T, Meloni F, Cobelli FD, Ferrero C, Maschio AD. Small hepatocellular carcinoma treated with percutaneous RF ablation: MR imaging follow-up. *AJR* 1999;173:1225-1229
15. Boaz TL, Lewin JS, Chung YC, Duerk JL, Clampitt ME, Haaga JR. MR monitoring of MR-guided radiofrequency thermal ablation of normal liver in an animal model. *J Magn Reson Imaging* 1998;8:64-69
16. Goldberg SN, Gazelle GS, Mueller PR. Thermal ablation therapy for focal malignacy: a unified approach to underlying principles, techniques, and diagnostic imaging guidance. *AJR* 2000; 174:323-331
17. Sanchez R, vanSonnenberg E, D'Agostino H et al. Percutaneous tissue ablation by radiofrequency thermal energy as a prelim to tumor ablation. *Min Inv Ther* 1993;2:299-305
18. Curley SA, Davidson BS, Fleming RY, et al. Laparoscopically guided bipolar radiofrequency ablation of areas of porcine liver. *Surg Endosc* 1997;11:729-733
19. Rossi S, Di Stasi M, Buscarini E, et al. Percutaneous RF interstitial thermal ablation in the treatment of hepatic cancer. *AJR* 1996;167:759-768
20. Solbiati L, Goldberg SN, Ierace T, et al. Radiofrequency ablation of hepatic metastases: postprocedural assessment with a US microbubble contrast agent-early experience. *Radiology* 1999; 211:643-649
21. Steiner P, Botnar R, Goldberg SN, Gazelle GS, Debatin JF. Monitoring of radiofrequency tissue ablation in an interventional MR environment: preliminary ex vivo and in vivo results. *Invest Radiol* 1997;32:671-678
22. Fullerton G, Stark D, Bradley W. *Physiologic basis of magnetic relaxation.* In *Magnetic resonance imaging,* 2nd ed. St. Louis: Mosby Year Book;1992:95-99
23. Darkazanili A, Hynynen K, Unger E, Schenck J. On-line monitoring of ultrasonic surgery with MR imaging. *J Magn Reson Imaging* 1993;3:509-514
24. McGahan JP, Brock JM, Tesluk H, et al. Hepatic ablation with use of radio-frequency electrocautery in the animal model. *J Vasc Interv Radiol* 1992;3:291-297
25. Raman SS, Lu DSK, Vodopich DJ, Sayre J, Lassman C. Creation of radiofrequency lesions in a porcine model: correlation with sonography, CT, and histopathology. *AJR* 2000;175: 1253-1258
26. Castro DJ, Abergel PR, Johnston KJ, et al. Wound healing: biological effects of Nd:YAG laser on collagen metabolism in pig skin in comparison to thermal burn. *Ann Plast Surg* 1983;11: 131-140